

High-temperature structural study of six olivines

GEORGE A. LAGER

Department of Geosciences, Rider College
Lawrenceville, New Jersey 08648

AND E. P. MEAGHER

Department of Geological Sciences
University of British Columbia
Vancouver, Canada V6T 1W5

Abstract

Single-crystal X-ray intensity data have been collected with a manual diffractometer utilizing flat-cone geometry for Ni-olivine, Ni_2SiO_4 , (25°, 300°, 600°, and 900°C), monticellite, $\text{Ca}_{1.00}\text{Mg}_{0.93}\text{Fe}_{0.07}\text{SiO}_4$, (25°, 335°, 615°, and 795°C), and glaucochroite, $\text{Ca}_{0.98}\text{Mn}_{0.87}\text{Mg}_{0.10}\text{Zn}_{0.05}\text{SiO}_4$, (25°, 300°, 600°, and 800°C). Weighted refinements with anisotropic temperature factors resulted in residual (R) factors ranging from 0.026 to 0.048. Examination of these data, together with published data from high-temperature refinements of forsterite, hortonolite, and fayalite, indicates that the olivine structure expands primarily as a result of bond-length expansions in $M(1)$ and $M(2)$ octahedra. Mean Mg–O distances exhibit the greatest thermal expansions while the mean M –O distances in Fe-containing olivines generally exhibit the smallest expansions. The $M(2)$ cation position in all six olivines is temperature-dependent. With increasing temperature, the cation is displaced in a direction away from the triangle of shared edges. The magnitude of this displacement, measured relative to the centroid of coordinating oxygens, is greatest for non-transition metal cations (Mg^{2+} , Ca^{2+}).

Introduction

Since the original determination of the crystal structure of olivine by Bragg and Brown (1926), structure refinements have been carried out on a variety of olivine-type minerals¹ at both room and elevated temperatures. Of the more recent investigations at room temperature, Brown (1970) refined the structures of several olivines ranging in composition from Ni_2SiO_4 to $\gamma\text{-Ca}_2\text{SiO}_4$, while other refinements include those of Wenk and Raymond (1973) (Fa_{01} , Fa_{10} , Fa_{30} , Fa_{32}); Ghose and Wan (1974) ($\text{Co}_{1.10}\text{Mg}_{0.90}\text{SiO}_4$); Brown and Prewitt (1973) (Fa_{18} , Fa_{29}); Rajamani *et al.* (1975) ($\text{Ni}_{1.03}\text{Mg}_{0.97}\text{SiO}_4$). Crys-

tal-structure refinements of data collected at high temperature have been limited to compositions ranging from forsterite to fayalite, *e.g.* Brown and Prewitt (1973) (Fa_{30}); Smyth and Hazen (1973) (Fo_{100} and $\text{Mg}_{0.75}\text{Fe}_{1.10}\text{Mn}_{0.15}\text{SiO}_4$); Smyth (1975) (Fa_{100}); and Hazen (1976) (Fo_{100}).

In the present investigation, the crystal structures of Ni-olivine (Ni_2SiO_4), monticellite ($\text{Ca}_{1.00}\text{Mg}_{0.93}\text{Fe}_{0.07}\text{SiO}_4$), and glaucochroite ($\text{Ca}_{0.98}\text{Mn}_{0.87}\text{Mg}_{0.10}\text{Zn}_{0.05}\text{SiO}_4$) have been refined with data collected at temperatures ranging from 25° to 900°C. These new high-temperature data are examined together with data from the refinements of forsterite (Smyth and Hazen, 1973), hortonolite (Brown and Prewitt, 1973), and fayalite (Smyth, 1975) in order to characterize the temperature dependence of the olivine-type structure. In a subsequent paper, three-dimensional strain theory will be used to examine the thermal expansion of the polyhedra within these structures (Lager and Meagher, 1975).

¹ In this study, the term olivine-type refers not only to the forsterite (Mg_2SiO_4)-fayalite (Fe_2SiO_4) group but to all silicates isostructural with forsterite/fayalite. Ni_2SiO_4 and $\gamma\text{-Ca}_2\text{SiO}_4$ represent end members in this group of minerals with respect to the size of the octahedral cations. Ni^{2+} and Ca^{2+} are, respectively, the smallest and largest cations that have been found to date to fully occupy the octahedral sites.

Table 1. Chemical analyses for monticellite and glaucochroite

Oxide	Weight % Oxides	
	Monticellite	Glaucochroite
MgO	23.61(20)*	22.27(20)
SiO ₂	37.28(26)	33.40(20)
CaO ²	35.37(24)	29.99(22)
MnO	-	33.29(24)
ZnO	-	2.35(35)
FeO	3.22(18)	-
Total	99.48	101.30
Number of Atoms Per 4 Oxygens		
Mg	0.936	0.103
Si	0.992	1.000
Ca	1.008	0.979
Mn	-	0.866
Zn	-	0.052
Fe	0.071	-

* The numbers in parentheses in this and subsequent tables are estimated standard deviations and refer to the last decimal place cited.

Experimental details

Specimen description and data collection

With the exception of monticellite, the crystals used in this study were the same as those examined by Brown (1970). The monticellite crystal from Crestmore, California, was kindly donated for study by the Department of Geological Sciences at the University of British Columbia.

The chemistry of the synthetic crystal of Ni-olivine has been reported as pure Ni₂SiO₄ (Brown, 1970). The natural crystals of monticellite and glaucochroite were chemically analyzed on a ARL-SEMQ electron microprobe. The data were reduced using the empirical correction factors determined by Bence and Albee (1968). Compositions reported represent the average of approximately 15 crystals. The mean chemical analyses and the estimated standard deviations of the mean values are presented in Table 1.

Equidimensional crystals approximately 0.05–0.10 mm in diameter were oriented parallel to either *c* or *a* in tapered fused-silica capillaries which were then cemented to a platinum wire attached to the goniometer. In the case of glaucochroite, heating experiments prior to data collection indicated probable alteration. As a result, the crystal was mounted directly on a tapered silica capillary, using a high-temperature cement composed of Sauereisen binder no. 29 and powdered kaowool filler.² The crystal,

mounted on the capillary, was then inserted into a larger capillary of approximately 0.3 mm in diameter which was flushed with hydrogen gas, evacuated with a vacuum pump, and sealed under vacuum using an oxyacetylene mini-torch.

The furnace used in this study was modified from the design of Foit and Peacor (1967). The furnace, which requires flat-cone geometry, has been adapted to a Weissenberg camera for space-group and cell-dimension work and to a manually-operated Supper-Weissenberg diffractometer for three-dimensional single-crystal intensity data collection. The diffractometer is used with Zr-filtered Mo-radiation and a pulse-height discriminator. The furnace temperature was calibrated with a Pt/Pt-13% Rh thermocouple which was centered in the furnace in place of the sample before each high-temperature run. The estimated accuracy of the temperature, based on the thermocouple measurements and the melting points of Zn (419°C) and KBr (730°C), is ± 15°C.

The unit-cell parameters for each olivine at high temperature were determined from a least-squares refinement of film data collected with a large-diameter cassette built for the standard Weissenberg camera (Meagher, 1975). In addition to the 0-level Weissenberg photographs used for cell-dimension work, upper-level flatcone photographs were also recorded at each temperature. These photographs were

Table 2. Residual-factors and number of observations for refinements of Ni-olivine, monticellite, and glaucochroite

Ni-olivine	Number of Observations	R*	R _w **
25°	228	0.037	0.045
300°	226	0.032	0.048
600°	233	0.027	0.036
900°	230	0.027	0.036
Monticellite			
25°	223	0.030	0.039
335°	228	0.025	0.032
625°	226	0.028	0.026
795°	220	0.029	0.032
Glaucochroite			
25°	233	0.024	0.026
300°	230	0.024	0.026
600°	213	0.030	0.033
800°	201	0.028	0.029

$$* R = \sum |F_{\text{obs}}| - |F_{\text{calc}}| / \sum |F_{\text{obs}}|$$

$$** R_w = [\sum w(|F_{\text{obs}}| - |F_{\text{calc}}|)^2 / \sum w F_{\text{obs}}^2]$$

² Babcock and Wilcox Refractories, Burlington, Ontario.

Table 4. Positional parameters and isotropic temperature factors for the atoms in Ni-olivine, monticellite, and glaucochroite

		Ni-Olivine				Glaucochroite					
Atom	Parameter	25°C	300°C	600°C	900°C	Atom	Parameter	25°C	300°C	600°C	800°C
M(1)	x	0.0	0.0	0.0	0.0	M(1)	x	0.0	0.0	0.0	0.0
	y	0.0	0.0	0.0	0.0		y	0.0	0.0	0.0	0.0
	z	0.0	0.0	0.0	0.0		z	0.0	0.0	0.0	0.0
	B	0.34(2)	0.64(2)	0.97(2)	1.43(2)		B	0.54(3)	1.16(3)	1.95(4)	2.51(4)
M(2)	< μ >	0.066	0.090	0.111	0.135		< μ >	0.083	0.121	0.157	0.178
	x	0.9924(2)	0.9925(3)	0.9922(2)	0.9919(2)	M(2)	x	0.9803(5)	0.9797(5)	0.9805(6)	0.9806(6)
	y	0.2738(1)	0.2745(1)	0.2746(1)	0.2750(1)		y	0.2780(1)	0.2789(1)	0.2797(2)	0.2802(2)
	z	0.25	0.25	0.25	0.25		z	0.25	0.25	0.25	0.25
Si	B	0.34(2)	0.66(2)	1.01(2)	1.47(2)		B	0.41(4)	0.85(4)	1.48(5)	1.90(5)
	< μ >	0.066	0.091	0.113	0.136		< μ >	0.072	0.104	0.137	0.155
	x	0.4276(4)	0.4272(5)	0.4276(4)	0.4277(4)	Si	x	0.4161(5)	0.4150(5)	0.4156(7)	0.4153(7)
	y	0.0944(2)	0.0947(3)	0.0941(2)	0.0943(2)		y	0.0868(2)	0.0875(2)	0.0880(3)	0.0895(3)
	z	0.25	0.25	0.25	0.25		z	0.25	0.25	0.25	0.25
	B	0.29(3)	0.52(4)	0.70(3)	1.00(3)		B	0.39(5)	0.80(5)	1.30(7)	1.72(7)
O(1)	< μ >	0.061	0.081	0.094	0.113		< μ >	0.070	0.101	0.128	0.148
	x	0.7703(9)	0.7697(13)	0.7693(12)	0.7682(10)	O(1)	x	0.7466(14)	0.7452(14)	0.7429(18)	0.7378(19)
	y	0.0935(6)	0.0923(7)	0.0930(6)	0.0934(6)		y	0.0843(5)	0.0841(5)	0.0840(6)	0.0840(7)
	z	0.25	0.25	0.25	0.25		z	0.25	0.25	0.25	0.25
O(2)	B	0.53(8)	1.02(11)	1.18(10)	1.67(9)		B	0.61(12)	1.27(14)	1.83(18)	2.33(20)
	< μ >	0.082	0.114	0.122	0.145		< μ >	0.088	0.127	0.152	0.172
	x	0.2197(11)	0.2187(14)	0.2163(13)	0.2166(11)	O(2)	x	0.2305(14)	0.2277(14)	0.2312(20)	0.2311(19)
	y	0.4455(6)	0.4454(7)	0.4459(6)	0.4464(5)		y	0.4528(5)	0.4542(5)	0.4555(6)	0.4549(6)
O(3)	z	0.25	0.25	0.25	0.25		z	0.25	0.25	0.25	0.25
	B	0.36(8)	0.97(11)	1.07(10)	1.56(8)		B	0.60(6)	0.92(12)	1.80(18)	2.20(18)
	< μ >	0.068	0.111	0.116	0.141		< μ >	0.087	0.108	0.151	0.167
	x	0.2754(8)	0.2770(10)	0.2778(9)	0.2787(8)	O(3)	x	0.2818(9)	0.2827(9)	0.2819(11)	0.2831(12)
Si	y	0.1633(4)	0.1632(5)	0.1630(4)	0.1631(4)		y	0.1527(3)	0.1530(3)	0.1539(4)	0.1539(4)
	z	0.0310(10)	0.0324(12)	0.0328(11)	0.0333(9)		z	0.0493(6)	0.0500(6)	0.0519(8)	0.0526(8)
	B	0.50(6)	1.00(8)	1.36(7)	1.74(6)		B	0.58(9)	1.06(9)	1.74(12)	2.22(13)
	< μ >	0.080	0.113	0.131	0.148		< μ >	0.086	0.116	0.148	0.168
		Monticellite									
		25°C	335°C	615°C	795°C						
M(1)	x	0.0	0.0	0.0	0.0						
	y	0.0	0.0	0.0	0.0						
	z	0.0	0.0	0.0	0.0						
	B	0.29(1)	0.74(3)	1.42(4)	1.92(4)						
M(2)	< μ >	0.061	0.097	0.134	0.156						
	x	0.9771(3)	0.9764(2)	0.9759(3)	0.9753(3)						
	y	0.2766(1)	0.2774(1)	0.2781(1)	0.2789(1)						
	z	0.25	0.25	0.25	0.25						
Si	B	0.38(2)	0.88(2)	1.44(3)	1.93(3)						
	< μ >	0.069	0.106	0.135	0.156						
	x	0.4110(3)	0.4091(3)	0.4087(3)	0.4076(4)						
	y	0.0815(1)	0.0817(1)	0.0824(2)	0.0829(2)						
O(1)	z	0.25	0.25	0.25	0.25						
	B	0.28(3)	0.62(3)	1.07(3)	1.42(3)						
	< μ >	0.060	0.089	0.116	0.134						
	x	0.7460(9)	0.7434(8)	0.7428(10)	0.7398(10)						
O(2)	y	0.0768(4)	0.0776(4)	0.0785(5)	0.0785(5)						
	z	0.25	0.25	0.25	0.25						
	B	0.45(8)	1.24(8)	2.00(10)	2.66(11)						
	< μ >	0.075	0.125	0.159	0.184						
O(3)	x	0.2466(8)	0.2476(8)	0.2463(9)	0.2463(9)						
	y	0.4491(4)	0.4501(3)	0.4509(4)	0.4521(4)						
	z	0.25	0.25	0.25	0.25						
	B	0.54(7)	1.01(5)	1.47(8)	1.86(9)						
O(3)	< μ >	0.083	0.113	0.136	0.153						
	x	0.2725(6)	0.2738(6)	0.2731(6)	0.2729(7)						
	y	0.1466(3)	0.1473(3)	0.1476(3)	0.1479(3)						
	z	0.0451(7)	0.0472(6)	0.0472(7)	0.0477(8)						
	B	0.55(5)	1.02(5)	1.63(6)	2.12(6)						
	< μ >	0.083	0.114	0.144	0.164						

*Isotropic equivalents of the anisotropic temperature factors (Hamilton, 1959)

Approximately 250 symmetry non-equivalent reflections of $\sin \theta \leq 0.5$ were collected with a manual Weissenberg scintillation-counter diffractometer for Ni-olivine (25°, 300°, 600°, and 900°), monticellite (25°, 335°, 615°, and 795°), and glaucochroite (25°, 300°, 600°, and 800°). For each crystal, data were recollected at room temperature after heating to determine if any permanent changes had occurred as a result of the heating cycle. Each reflection was scanned and traced on a strip-chart recorder. Relative intensities were determined using an integration planimeter and reduced to $|F_{\text{obs}}|$ using a program which corrects for Lorentz and polarization effects. Examination of transmission factors and sets of symmetry-equivalent reflections for each crystal indicated negligible differential absorption. The small number of observable reflections reflects both the small size of the crystals and the geometric restrictions imposed by the design of the furnace and diffractometer. The latter factor imposed an upper limit on the value of the μ angle, which resulted in the loss of reflections of the type $l = 6$ for Ni-olivine and monticellite and $h = 5$ for glaucochroite.

Refinements

Full matrix least-squares refinements were calculated for each data set using a modified version of ORFLS (Busing *et al.*, 1962) and the neutral atomic

checked for systematic absences and found to be consistent with space group $Pbnm$ in all cases. With the exception of glaucochroite, the same crystal was used for cell parameters and intensity collection.

Table 5. Anisotropic temperature factor coefficients ($\times 10^4$) for Ni-olivine, monticellite, and glaucochroite

Atom	ij of β_{ij}	Ni-Olivine				Atom	Glaucochroite				
		25°C	300°C	600°C	900°C		25°C	300°C	600°C	800°C	
M(1)	11	55(5)	76(6)	104(5)	133(4)	M(1)	11	37(8)	117(7)	199(9)	246(10)
	22	6(1)	19(1)	29(1)	39(1)		22	15(1)	27(1)	46(1)	60(1)
	33	20(9)	34(9)	56(11)	100(6)		33	31(2)	59(2)	94(3)	121(4)
	12	-0(11)	-2(2)	-5(2)	-4(2)		12	-3(2)	-5(2)	-12(3)	-14(4)
	13	-2(2)	-5(3)	-7(3)	-12(3)		13	-7(4)	-25(4)	-29(5)	-46(6)
	23	-3(1)	-5(2)	-8(1)	-9(1)		23	-3(1)	-5(1)	-10(2)	-11(2)
M(2)	11	60(5)	84(6)	125(5)	162(5)	M(2)	11	39(11)	111(9)	175(12)	239(14)
	22	1(1)	15(1)	22(1)	29(1)		22	10(1)	16(1)	27(1)	34(1)
	33	32(5)	43(6)	71(5)	120(5)		33	20(3)	40(3)	81(4)	96(4)
	12	-1(1)	-1(2)	1(2)	1(1)		12	-1(2)	-2(2)	6(3)	-0(4)
Si	11	51(8)	36(10)	54(9)	76(7)	Si	11	23(14)	93(13)	148(18)	166(19)
	22	2(1)	12(2)	16(2)	24(1)		22	9(1)	17(2)	27(2)	35(2)
	33	25(8)	51(11)	66(10)	91(8)		33	30(5)	37(4)	64(6)	101(7)
	12	1(3)	1(3)	8(3)	-0(2)		12	-5(3)	-3(3)	-6(4)	-12(5)
O(1)	11	26(17)	79(25)	108(22)	105(19)	O(1)	11	36(33)	128(35)	146(44)	239(49)
	22	11(5)	22(6)	35(5)	48(5)		22	16(4)	28(5)	39(7)	56(7)
	33	65(23)	104(32)	79(28)	144(24)		33	41(12)	71(13)	123(18)	106(18)
	12	-3(8)	1(12)	-1(10)	-5(8)		12	-7(11)	4(11)	12(15)	23(17)
O(2)	11	85(20)	93(26)	171(24)	204(21)	O(2)	11	52	57(31)	223(46)	231(46)
	22	3(4)	10(5)	18(5)	22(4)		22	8(3)	22(4)	31(6)	34(6)
	33	14(24)	118(36)	65(26)	133(25)		33	53(11)	66(11)	99(15)	154(18)
	12	7(7)	17(9)	25(9)	21(7)		12	10(9)	4(8)	2(12)	-17(13)
O(3)	11	73(14)	98(18)	148(16)	181(15)	O(3)	11	56(23)	106(23)	174(29)	250(32)
	22	12(3)	35(4)	35(4)	48(3)		22	14(3)	25(3)	31(4)	52(5)
	33	25(16)	47(21)	91(19)	110(16)		33	29(7)	53(8)	114(11)	93(10)
	12	-2(5)	-8(7)	5(6)	-1(6)		12	2(5)	6(6)	-1(7)	9(8)
	13	10(11)	-4(14)	-9(13)	-18(11)		13	1(9)	5(10)	4(14)	0(15)
	23	1(6)	13(7)	5(6)	11(6)		23	3(4)	0(4)	12(5)	18(5)
Monticellite											
M(1)		25°C	335°C	615°C	795°C						
	11	24(7)	92(7)	157(8)	166(8)						
	22	6(1)	17(1)	33(2)	41(2)						
	33	22	31(9)	67(11)	130(17)						
	12	-3(2)	-5(2)	-12(3)	-15(3)						
	13	-7(5)	-23(5)	-28(6)	-42(7)						
M(2)	11	58(6)	117(5)	175(6)	215(7)						
	22	9(1)	15(1)	24(1)	32(1)						
	33	11(5)	49(6)	88(6)	130(10)						
	12	1(2)	3(2)	7(2)	7(2)						
Si	11	24(7)	41(6)	83(7)	107(7)						
	22	7(1)	14(1)	22(1)	29(1)						
	33	18(7)	46(7)	83(8)	108(11)						
	12	-2(2)	2(2)	-2(2)	-3(3)						
O(1)	11	26(16)	32(15)	88(18)	137(21)						
	22	20(4)	32(4)	49(5)	61(5)						
	33	9(19)	112(19)	163(23)	218(28)						
	12	-5(6)	-8(6)	-6(7)	-0(8)						
O(2)	11	27(17)	117(18)	149(20)	147(20)						
	22	4(3)	14(3)	23(4)	30(4)						
	33	71(20)	75(18)	112(20)	162(23)						
	12	6(6)	10(6)	11(7)	1(7)						
O(3)	11	44(12)	95(11)	175(13)	232(14)						
	22	16(2)	24(2)	33(2)	38(3)						
	33	29(11)	60(10)	96(12)	135(14)						
	12	8(4)	-0(4)	2(5)	9(5)						
	13	-8(9)	14(8)	-1(10)	-5(11)						
	23	2(4)	10(4)	11(5)	16(5)						
	$*\beta_{13} = \beta_{23} = 0$ for M(2), Si, O(1), and O(2).										

scattering curves of Doyle and Turner (1968). Starting positional and thermal parameters, isotropic temperature factors and scale factors were calculated utilizing unit weights. Upon convergence, the isotropic temperature factors were converted to the an-

isotropic form and the refinement was continued with a modified version of the Cruickshank weighting scheme (Cruickshank, 1965).

In the refinement of Ni-olivine, large negative differences $|F_{\text{obs}}| - |F_{\text{calc}}|$ for the intense low-angle reflections were noted. An extinction correction was then applied to the data by minimizing the function $\sum w_i [F_{o,i} - S \cdot F_{c,i}/(1 + \alpha \cdot I_i)]^2$, where I_i are the uncorrected intensities, α the extinction coefficient, S the scale factor, and w_i the weights.

Refinements of each olivine at room temperature with anisotropic temperature factors resulted in a few non-positive definite temperature factors. In the case of Ni-olivine, a strong correlation was noted between a scale factor and the anisotropic temperature factor coefficient, β_{33} , of M(1). When this scale factor was held constant during the final refinement, β_{33} refined to a positive value. The parameter β_{33} for M(1) in monticellite and β_{11} for O(2) in glaucochroite were locked at 22×10^{-4} and 52×10^{-4} respectively, following refinements to negative values. The positional parameters obtained in refinements which resulted in non-positive β 's were identical to those obtained in refinements in which scale factors or temperature factors had been locked.

The final weighted (R_w) and unweighted residuals (R) for the anisotropic refinements and the number of observations used in each refinement are presented in

Table 6. Magnitudes and orientations of the principal axes of the thermal vibration ellipsoids for the atoms in Ni-olivine, monticellite, and glaucochroite

Olivine	T°C	i of r _i	r _i (Å)	O(1)			O(2)			Si				
				Angle (°) of r _i with			Angle (°) of r _i with			Angle (°) of r _i with				
				+a	+b	+c	r _i (Å)	+a	+b	+c	r _i (Å)	+a	+b	+c
Ni-Olivine	25	1	0.053(19)	14(38)	76(33)	90	0.033(34)	101(11)	11(11)	90	0.061(21)	108(19)	99(36)	20(25)
		2	0.075(16)	76(38)	166(38)	90	0.048(44)	90	90	180	0.080(10)	96(31)	168(30)	101(34)
		3	0.106(19)	90	90	0	0.100(11)	11(11)	79(11)	90	0.093(8)	19(19)	99(28)	73(20)
	300	1	0.095(15)	10(73)	100(73)	90	0.052(25)	118(12)	28(12)	90	0.083(21)	90(27)	109(12)	19(12)
		2	0.106(15)	100(73)	170(73)	90	0.114(13)	152(12)	118(12)	90	0.104(10)	167(11)	103(15)	94(26)
		3	0.135(21)	90	90	0	0.145(22)	90	90	0	0.142(9)	103(11)	23(10)	71(10)
	600	1	0.111(12)	3(24)	87(24)	90	0.081(15)	116(7)	26(7)	90	0.119(10)	123(27)	63(20)	135(31)
		2	0.119(21)	90	90	180	0.108(22)	90	90	180	0.134(9)	39(39)	92(68)	129(37)
		3	0.135(11)	93(24)	3(24)	90	0.150(10)	26(7)	64(7)	90	0.139(8)	72(57)	27(19)	70(54)
	900	1	0.110(10)	5(9)	85(9)	90	0.100(10)	111(7)	21(6)	90	0.130(9)	60(18)	108(11)	36(14)
		2	0.159(8)	85(9)	175(9)	90	0.155(14)	90	90	180	0.148(6)	146(19)	115(18)	69(17)
		3	0.161(14)	90	90	0	0.160(8)	21(6)	69(6)	90	0.165(6)	103(14)	32(15)	62(12)
Monticellite	25	1	0.044(44)	90	90	0	0.038(26)	131(28)	41(28)	90	0.059(13)	36(20)	110(10)	62(25)
		2	0.053(18)	172(9)	98(9)	90	0.067(15)	139(28)	131(28)	90	0.082(12)	62(25)	96(20)	151(25)
		3	0.112(10)	98(9)	8(9)	90	0.121(17)	90	0	0.104(7)	69(12)	21(10)	86(19)	
	335	1	0.060(15)	7(5)	83(5)	90	0.088(11)	114(12)	24(12)	90	0.093(9)	54(19)	66(12)	134(13)
		2	0.142(8)	83(5)	173(5)	90	0.123(9)	156(12)	114(12)	90	0.111(7)	38(20)	119(16)	68(15)
		3	0.153(13)	90	90	0	0.125(15)	90	90	0	0.133(6)	79(11)	40(12)	52(10)
	615	1	0.102(11)	4(5)	86(5)	90	0.114(10)	122(15)	32(15)	90	0.128(8)	90(19)	48(11)	137(12)
		2	0.177(8)	86(5)	176(5)	90	0.140(9)	148(15)	122(15)	90	0.144(5)	171(19)	10(23)	81(19)
		3	0.185(13)	90	90	0	0.153(14)	90	90	0	0.156(7)	84(23)	42(11)	49(12)
	795	1	0.128(10)	0(5)	90(5)	90	0.133(9)	10(77)	100(77)	90	0.140(7)	106(10)	37(8)	123(9)
		2	0.197(9)	90(5)	180(5)	90	0.138(9)	100(77)	170(77)	90	0.168(5)	161(14)	98(18)	73(20)
		3	0.214(14)	90	90	0	0.185(13)	90	90	0	0.180(7)	81(24)	54(9)	38(14)
Glaucochroite	25	1	0.062(32)	17(25)	73(25)	90	0.053(25)	128(13)	38(13)	90	0.077(10)	93(91)	107(29)	17(21)
		2	0.094(14)	90	90	180	0.092(14)	142(13)	128(13)	90	0.082(17)	167(43)	77(44)	89(20)
		3	0.102(14)	107(25)	17(25)	90	0.106(11)	90	90	0	0.097(9)	77(36)	22(28)	73(21)
	300	1	0.124(11)	90	90	0	0.082(23)	8(19)	98(19)	90	0.104(8)	118(49)	82(24)	29(53)
		2	0.124(16)	157(68)	67(68)	90	0.119(10)	90	90	180	0.113(10)	39(40)	114(29)	61(54)
		3	0.134(12)	67(68)	23(68)	90	0.119(11)	82(19)	8(19)	90	0.129(7)	65(26)	26(27)	85(16)
	600	1	0.129(20)	22(26)	112(26)	90	0.140(12)	94(25)	4(25)	90	0.131(9)	84(27)	32(12)	121(10)
		2	0.162(14)	112(26)	158(26)	90	0.146(11)	90	90	180	0.147(12)	173(26)	83(26)	89(23)
		3	0.163(12)	90	90	0	0.166(17)	4(25)	86(25)	90	0.165(8)	86(23)	59(11)	31(10)
	800	1	0.151(13)	90	90	0	0.138(14)	63(17)	27(17)	90	0.132(9)	86(10)	113(6)	24(7)
		2	0.160(17)	32(19)	122(19)	90	0.177(15)	27(17)	117(17)	90	0.174(10)	158(21)	72(21)	78(11)
		3	0.200(14)	58(19)	32(19)	90	0.183(11)	90	90	0	0.193(8)	68(22)	30(15)	70(7)

Table 2. The observed and calculated structure amplitudes are compared in Table 3.³ The final positional parameters and isotropic equivalents of the anisotropic temperature factors are given in Table 4, the anisotropic temperature-factor coefficients in Table 5, and the resulting magnitude and orientation of the principal axes of the thermal vibration ellipsoids are presented in Table 6. Positional parameters obtained from refinements of data collected before and after heating are statistically identical and are within 2σ of those reported by Brown (1970).

The interatomic distances and angles and their estimated standard deviations were calculated with the program ORFFE (Busing *et al.*, 1964) and are tabulated in Tables 7 and 8. The interatomic distances are

³ To receive a copy of Table 3, order document number AM-78-064 from the Business Office, Mineralogical Society of America, Suite 1000 lower level, 1909 K Street NW, Washington, DC 20006. Please remit \$1.00 in advance for the microfiche.

uncorrected for thermal motion and represent distances between mean atomic positions.

The thermal expansion of selected parameters in this study has been represented by a linear thermal expansion coefficient defined as

$$\alpha = \frac{1}{l_{25}} \frac{(l_T - l_{25})}{(T - 25)} \quad (1)$$

where l_{25} and l_T are the lengths of selected parameters at 25°C and at some higher temperature T . In this study, the quantity $(l_T - l_{25})/(T - 25)$ is the slope determined from a simple linear regression of l versus T . Although some of the trends may not be linear, deviations from linearity are small enough to warrant simplification by this technique for comparative purposes.

Olivine structure

A drawing of a portion of the olivine structure projected on (100) is given in Figure 1. The pre-

Table 6. continued

Olivine	T°C	i of r _i	M(1)						M(2)						Si		
			Angle (°) of r _i with			Angle (°) of r _i with			Angle (°) of r _i with			Angle (°) of r _i with			Angle (°) of r _i with		
			r _i (A)	+a	+b	+c	r _i (A)	+a	+b	+c	r _i (A)	+a	+b	+c	r _i (A)	+a	+b
Ni-Olivine	25	1	0.048(7)	88(4)	42(30)	48(21)	0.024(11)	87(3)	3(3)	90	0.030(12)	93(8)	3(8)	90			
		2	0.064(7)	86(9)	132(30)	42(29)	0.074(6)	90	90	180	0.064(11)	90	90	180			
		3	0.079(4)	5(8)	89(6)	95(8)	0.083(4)	3(3)	93(3)	90	0.076(6)	3(8)	87(8)	90			
	300	1	0.074(9)	75(11)	68(8)	27(12)	0.087(6)	90	90	0	0.062(9)	6(18)	96(18)	90			
		2	0.093(4)	162(11)	94(16)	72(11)	0.089(4)	99(14)	171(14)	90	0.080(6)	96(18)	174(18)	90			
		3	0.102(3)	100(14)	22(7)	110(10)	0.098(4)	9(14)	99(14)	90	0.096(10)	90	90	0			
	600	1	0.092(8)	69(11)	68(5)	32(11)	0.108(2)	96(9)	6(9)	90	0.072(7)	150(8)	60(8)	90			
		2	0.111(3)	157(9)	91(10)	67(10)	0.113(4)	90	90	180	0.098(5)	120(8)	150(8)	90			
		3	0.127(2)	100(6)	22(5)	110(7)	0.120(2)	6(9)	84(9)	90	0.109(8)	90	90	0			
	900	1	0.117(2)	38(7)	71(3)	58(6)	0.124(2)	96(6)	6(6)	90	0.093(5)	0(8)	90(8)	90			
		2	0.134(3)	52(7)	116(8)	131(4)	0.137(2)	174(6)	96(6)	90	0.113(3)	90(8)	180(8)	90			
		3	0.151(2)	89(4)	33(6)	123(6)	0.147(3)	90	90	0	0.128(5)	90	90	0			
Monticellite	25	1	0.043(10)	37(13)	63(14)	67(11)	0.047(12)	90	90	0	0.050(8)	21(19)	69(19)	90			
		2	0.066(7)	64(39)	153(17)	81(70)	0.073(4)	76(16)	166(16)	90	0.061(12)	90	90	180			
		3	0.070(4)	115(37)	93(69)	25(28)	0.083(4)	14(16)	76(16)	90	0.066(6)	111(19)	21(19)	90			
	335	1	0.066(11)	60(7)	81(6)	31(8)	0.096(3)	100(5)	10(5)	90	0.070(6)	7(7)	97(7)	90			
		2	0.102(4)	107(13)	153(12)	70(8)	0.101(6)	90	90	180	0.096(4)	97(7)	173(7)	90			
		3	0.116(4)	145(7)	65(13)	66(9)	0.118(3)	10(5)	80(5)	90	0.098(8)	90	90	0			
	615	1	0.106(7)	57(8)	81(6)	35(9)	0.122(2)	107(4)	17(4)	90	0.099(4)	8(9)	82(9)	90			
		2	0.136(4)	121(10)	135(8)	61(8)	0.136(5)	90	90	180	0.117(3)	82(9)	172(9)	90			
		3	0.156(4)	131(6)	46(8)	72(7)	0.146(3)	17(4)	73(4)	90	0.132(6)	90	90	0			
	795	1	0.120(5)	34(4)	70(4)	63(6)	0.140(2)	108(5)	18(5)	90	0.113(4)	7(7)	83(7)	90			
		2	0.164(4)	81(12)	155(9)	68(15)	0.162(2)	162(5)	108(5)	90	0.135(3)	83(7)	173(7)	90			
		3	0.178(7)	123(7)	76(16)	36(14)	0.165(1)	90	90	0	0.151(8)	90	90	0			
Glaucocroite	25	1	0.061(8)	29(10)	78(6)	64(9)	0.066(4)	90	90	0	0.047(17)	22(13)	68(13)	90			
		2	0.083(4)	61(10)	107(9)	146(10)	0.068(9)	172(20)	98(20)	90	0.079(6)	68(13)	158(13)	90			
		3	0.099(3)	93(7)	21(7)	111(7)	0.081(4)	98(20)	8(20)	90	0.080(6)	90	90	0			
	300	1	0.094(4)	53(3)	75(3)	41(3)	0.093(3)	90	90	0	0.090(5)	90	90	0			
		2	0.132(3)	52(44)	139(62)	103(43)	0.100(3)	98(10)	172(10)	90	0.101(6)	127(32)	143(32)	90			
		3	0.134(3)	59(49)	53(64)	128(19)	0.117(5)	8(10)	98(10)	90	0.110(6)	143(32)	53(32)	90			
	600	1	0.125(4)	58(3)	70(3)	39(3)	0.129(4)	108(10)	18(10)	90	0.118(5)	90	90	0			
		2	0.166(4)	39(8)	79(13)	127(4)	0.133(3)	90	90	180	0.126(6)	127(24)	143(24)	90			
		3	0.177(3)	110(11)	23(7)	99(8)	0.149(5)	18(10)	72(10)	90	0.140(6)	143(24)	53(24)	90			
	800	1	0.137(4)	54(3)	74(2)	41(3)	0.144(3)	90	90	0	0.135(7)	37(13)	53(13)	90			
		2	0.190(3)	41(6)	81(12)	130(3)	0.148(3)	91(8)	179(8)	90	0.148(5)	90	90	180			
		3	0.201(3)	108(10)	19(7)	97(8)	0.172(5)	1(8)	91(8)	90	0.158(5)	127(13)	37(13)	90			

dominant structural feature is the zigzag chain of M(1) and M(2) octahedra parallel to *c*. M(1) octahedra, which possess $\bar{1}$ symmetry, share six oxygen-oxygen edges with adjacent polyhedra: two edges are shared with M(1) octahedra, two with M(2) octahedra, and two with Si tetrahedra. M(2) octahedra possess *m* symmetry and share a triangle of edges: two edges are shared with M(1) octahedra and one is shared with a Si tetrahedron. Si tetrahedra, one of which is shown in Figure 1, link octahedral chains in adjacent layers along *a*.

For the olivines considered in this study, M(1) and M(2) octahedra have been assigned the following cation occupancies respectively: hortonolite— $Mg_{0.675}Fe_{0.325}$, $Mg_{0.705}Fe_{0.285}$ (Brown and Prewitt, 1973); monticellite— $Mg_{0.93}Fe_{0.07}$, $Ca_{1.00}$; glaucocroite— $Mn_{0.85}Mg_{0.10}Zn_{0.05}$, $Ca_{0.98}Mn_{0.02}$ (Brown, 1970). The reader is referred to Birle *et al.* (1968) and Brown (1970) for a more detailed discussion of the

crystal structures and phase relations in the olivine group of minerals.

Polyhedral expansions

Si tetrahedra

The mean Si–O distances in the three olivines refined in this study remain relatively constant with heating. The largest change with temperature is observed in glaucocroite (Table 7) where the mean distance decreases from 1.640 to 1.629 Å over the temperature range 25° → 800°C. This decrease in the Si–O distance may not be realistic, however, since corrections have not been made for the increased thermal motion at high temperatures. The mean distances in forsterite, hortonolite, and fayalite show a similar response with temperature.

The mean oxygen–oxygen distance in the Ni-olivine tetrahedron remains essentially constant with

Table 7. Interatomic distances (Å) in Ni-olivine, monticellite, and glaucochroite

I. Ni-Olivine					II. Monticellite				
	25°C	300°C	600°C	900°C		25°C	335°C	615°C	795°C
Tetrahedron					Tetrahedron				
[1] Si-O(1)	1.620(5)	1.625(6)	1.627(6)	1.626(5)	[1] Si-O(1)	1.617(5)	1.617(5)	1.621(5)	1.614(6)
[1] Si-O(2)	1.660(6)	1.666(7)	1.657(6)	1.661(6)	[1] Si-O(2)	1.656(4)	1.651(4)	1.651(5)	1.645(5)
[2] Si-O(3)	1.637(5)	1.630(7)	1.634(6)	1.635(5)	[2] Si-O(3)	1.637(4)	1.629(4)	1.633(4)	1.632(5)
<Si-O>	1.639	1.638	1.638	1.639	<Si-O>	1.637	1.632	1.635	1.630
[1] O(1)-O(2)	2.758(7)	2.755(9)	2.754(8)	2.759(7)	[1] O(1)-O(2)	2.768(6)	2.767(6)	2.768(6)	2.753(7)
[2] O(1)-O(3)	2.765(6)	2.766(8)	2.766(7)	2.765(6)	[2] O(1)-O(3)	2.744(5)	2.730(5)	2.736(5)	2.730(6)
[2] O(2)-O(3)†	2.556(6)	2.560(8)	2.560(7)	2.564(6)	[2] O(2)-O(3)†	2.556(6)	2.556(5)	2.559(6)	2.554(6)
[1] O(3)-O(3)†	2.590(11)	2.582(15)	2.585(13)	2.588(11)	[1] O(3)-O(3)†	2.616(9)	2.599(8)	2.610(10)	2.611(10)
<O-O>	2.665	2.666	2.665	2.668	<O-O>	2.664	2.656	2.661	2.655
M(1) Octahedron					M(1) Octahedron				
[2] M(1)-O(1)	2.064(4)	2.067(5)	2.077(4)	2.089(4)	[2] M(1)-O(1)	2.186(3)	2.204(3)	2.217(4)	2.230(4)
[2] M(1)-O(2)	2.060(4)	2.071(5)	2.083(4)	2.088(4)	[2] M(1)-O(2)	2.089(3)	2.090(3)	2.098(3)	2.100(3)
[2] M(1)-O(3)	2.111(4)	2.123(5)	2.131(4)	2.142(4)	[2] M(1)-O(3)	2.113(3)	2.131(3)	2.137(3)	2.144(4)
<M(1)-O>	2.078	2.087	2.097	2.106	<M(1)-O>	2.129	2.142	2.151	2.158
[2] O(1)-O(3)††	2.806(5)	2.824(8)	2.835(7)	2.850(6)	[2] O(1)-O(3)††	2.961(5)	2.979(5)	2.985(5)	3.002(6)
[2] O(1)-O(3)'	3.092(6)	3.096(8)	3.110(7)	3.127(6)	[2] O(1)-O(3)'	3.117(5)	3.150(5)	3.170(6)	3.182(6)
[2] O(1)-O(2)††	2.838(7)	2.849(10)	2.870(9)	2.882(7)	[2] O(1)-O(2)	2.830(6)	2.842(6)	2.859(7)	2.869(7)
[2] O(1)-O(2)'	2.992(6)	3.001(8)	3.012(7)	2.023(6)	[2] O(1)-O(2)'	3.204(8)	3.219(5)	3.235(5)	3.245(6)
[2] O(2)-O(3)'	3.297(7)	3.322(8)	3.347(7)	3.364(6)	[2] O(2)-O(3)'	3.334(5)	3.359(5)	3.376(5)	3.389(6)
[2] O(2)-O(3)†	2.556(6)	2.560(8)	2.560(7)	2.564(6)	[2] O(2)-O(3)†	2.556(6)	2.556(5)	2.559(6)	2.554(6)
<O-O>	2.930	2.942	2.956	2.968	<O-O>	3.000	3.018	3.031	3.040
M(2) Octahedron					M(2) Octahedron				
[1] M(2)-O(1)	2.105(5)	2.130(7)	2.131(6)	2.141(6)	[1] M(2)-O(1)	2.484(5)	2.496(4)	2.501(5)	2.519(5)
[1] M(2)-O(2)	2.043(6)	2.040(7)	2.044(6)	2.054(5)	[1] M(2)-O(2)	2.316(5)	2.330(4)	2.335(5)	2.344(5)
[2] M(2)-O(3)	2.172(5)	2.183(6)	2.193(5)	2.204(5)	[2] M(2)-O(3)	2.414(4)	2.421(4)	2.431(4)	2.449(4)
[2] M(2)-O(3)''	2.054(5)	2.062(6)	2.068(6)	2.073(5)	[2] M(2)-O(3)''	2.291(4)	2.301(4)	2.306(5)	2.309(5)
<M(2)-O>	2.100	2.110	2.116	2.125	<M(2)-O>	2.368	2.378	2.385	2.393
[2] O(1)-O(3)''	2.969(7)	2.995(8)	3.000(7)	3.009(6)	[2] O(1)-O(3)''	3.607(6)	3.613(5)	3.613(6)	3.620(6)
[2] O(1)-O(3)††	2.806(5)	2.824(8)	2.835(7)	2.850(6)	[2] O(1)-O(3)††	2.961(5)	2.979(5)	2.985(5)	3.002(6)
[2] O(2)-O(3)	3.146(6)	3.154(8)	3.170(6)	3.184(6)	[2] O(2)-O(3)	3.609(6)	3.620(2)	3.635(6)	3.651(6)
[2] O(2)-O(3)'''	2.895(7)	2.901(9)	2.901(8)	2.913(7)	[2] O(2)-O(3)'''	3.148(5)	3.171(5)	3.184(5)	3.199(6)
[1] O(3)-O(3)†	2.590(11)	2.582(15)	2.585(13)	2.588(11)	[1] O(3)-O(3)†	2.616(9)	2.599(8)	2.610(10)	2.611(10)
[2] O(3)-O(3)''	2.966(5)	2.980(6)	2.992(5)	3.002(5)	[2] O(3)-O(3)''	3.381(5)	3.485(4)	3.389(5)	3.392(5)
[1] O(3)''-O(3)'''	3.323(11)	3.351(15)	3.366(13)	3.383(11)	[1] O(3)''-O(3)'''	3.767(9)	3.810(8)	3.826(10)	3.843(11)
<O-O>	2.956	2.970	2.980	2.991	<O-O>	3.316	3.329	3.337	3.349

*The numbers in brackets refer to the multiplicity of the bond.
†-O edge shared between an octahedron and tetrahedron.

††-O edge shared between two octahedra.

increasing temperature (Table 7). In monticellite and glaucochroite there is a small decrease, which primarily reflects a decrease in the length of the unshared edges O(1)-O(2) and O(1)-O(3). These trends are similar to those observed in forsterite and hortonolite over similar temperature ranges.

M(1) and M(2) octahedra

The mean interatomic distances in the M(1) and M(2) octahedra (Table 7) for six olivines are plotted versus temperature in Figures 2 and 3 respectively. The thermal expansion coefficients of the mean M(1)-O distances (Table 9) can be ranked as follows: Mg-O (forsterite)⁴ ~ Mg-O (monticellite) ~ Mn-O

⁴ Although the forsterite data are best fitted by a second-degree polynomial, a simple linear regression has been used for comparative purposes.

~ Ni-O > Fe-O ~ (Mg,Fe)-O. The thermal-expansion coefficients for the mean M(2)-O distances are more closely grouped, with hortonolite possessing the smaller value and forsterite the larger. In general, mean Mg-O distances seem to exhibit the greatest thermal expansions, whereas the mean distances in the Fe-containing olivines exhibit the smallest expansions. This is in agreement with the results of the pyroxene high-temperature studies (Cameron *et al.*, 1973).

Thermal expansions of the oxygen-oxygen edges in the octahedra generally decrease in the order unshared > shared with octahedra >> shared with tetrahedra. In both M(1) and M(2), O-M-O angles opposite edges shared with Si tetrahedra show significant decreases with temperature. Concomitant increases occur in the angles associated with the opposite unshared edges.

Table 7. Continued.

	III. Glaucochroite			
	25°C	300°C	600°C	900°C
Tetrahedron				
[1] Si-O(1)	1.624(8)	1.626(8)	1.617(10)	1.599(11)
[1] Si-O(2)	1.659(6)	1.647(6)	1.653(8)	1.677(8)
[2] Si-O(3)	1.634(4)	1.629(4)	1.630(6)	1.619(6)
<Si-O>	1.640	1.633	1.633	1.629
[1] O(1)-O(2)	2.764(9)	2.744(9)	2.749(12)	2.738(13)
[2] O(1)-O(3)	2.737(7)	2.733(7)	2.733(9)	2.712(10)
[2] O(2)-O(3)†	2.582(5)	2.575(6)	2.574(7)	2.583(7)
[1] O(3)-O(3)†	2.604(7)	2.602(8)	2.588(11)	2.583(11)
<O-O>	2.664	2.660	2.659	2.652
M(1) Octahedron				
[2] M(1)-O(1)	2.251(5)	2.259(5)	2.273(6)	2.292(6)
[2] M(1)-O(2)	2.160(4)	2.169(5)	2.163(6)	2.169(6)
[2] M(1)-O(3)	2.218(4)	2.229(4)	2.243(5)	2.253(5)
<M(1)-O>	2.210	2.219	2.226	2.238
[2] O(1)-O(3)††	3.032(8)	3.048(8)	3.061(10)	3.095(11)
[2] O(1)-O(3)'	3.282(6)	3.294(6)	3.319(8)	3.328(8)
[2] O(1)-O(2)	2.958(9)	2.974(9)	2.969(12)	3.004(12)
[2] O(1)-O(2)'	3.271(6)	3.281(3)	3.296(4)	3.301(5)
[2] O(2)-O(3)'	3.535(7)	3.565(7)	3.576(10)	3.590(10)
[2] O(2)-O(3)†	2.582(5)	2.575(6)	2.574(7)	2.583(7)
<O-O>	3.110	3.123	3.133	3.150
M(2) Octahedron				
[1] M(2)-O(1)	2.447(6)	2.465(6)	2.488(8)	2.511(9)
[1] M(2)-O(2)	2.305(6)	2.309(6)	2.327(8)	2.322(8)
[2] M(2)-O(3)	2.417(4)	2.429(4)	2.424(6)	2.435(6)
[2] M(2)-O(3)††	2.306(4)	2.308(4)	2.325(6)	2.329(6)
<M(2)-O>	2.366	2.375	2.386	2.394
[2] O(1)-O(3)††	3.522(6)	3.532(6)	3.544(8)	3.556(8)
[2] O(1)-O(3)'	3.032(8)	3.048(8)	3.061(10)	3.095(11)
[2] O(2)-O(3)	3.600(6)	3.619(6)	3.629(8)	3.630(8)
[2] O(2)-O(3)††	3.165(7)	3.169(7)	3.212(9)	3.215(10)
[1] O(3)-O(3)†	2.604(7)	2.602(8)	2.588(11)	2.583(11)
[2] O(3)-O(3)'	3.340(5)	3.345(5)	3.346(6)	3.357(6)
[1] O(3)-O(3)††	3.884(7)	3.902(8)	3.944(11)	3.960(12)
<O-O>	3.317	3.328	3.343	3.354

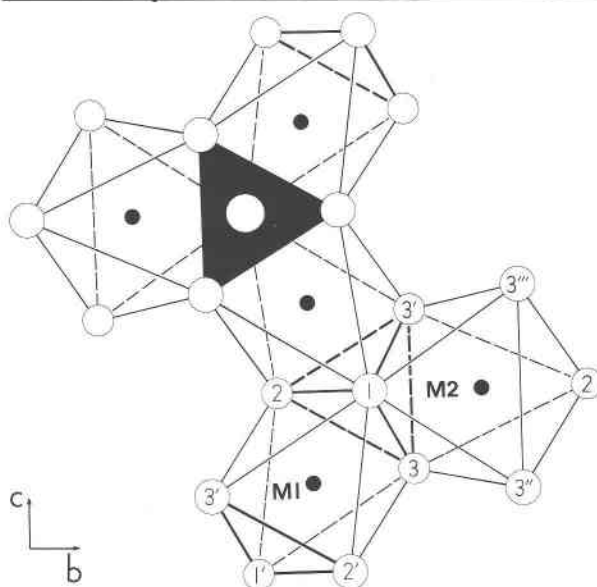


Fig. 1. A drawing of a portion of the olivine structure projected on (100). Bold-face lines indicate oxygen–oxygen edges which are shared between adjacent polyhedra. The M(1) cation labelled is located at $x = 0.50$, $y = 0.50$, and $z = 0.50$.

Table 8. Interatomic angles ($^{\circ}$) in Ni-olivine, monticellite, and glaucochroite

	Ni-Olivine			
	25°C	300°C	600°C	900°C
Tetrahedron				
*[1] O(1)-Si-O(2)	114.48(34)	113.69(43)	114.03(36)	114.19(33)
[2] O(1)-Si-O(3)	116.22(16)	116.32(25)	116.06(22)	115.94(19)
[2] O(2)-Si-O(3)†	101.67(19)	101.91(24)	102.14(22)	102.15(19)
[1] O(3)-Si-O(3)††	104.55(35)	104.72(47)	104.54(40)	104.60(36)
M(1) Octahedron				
[2] O(1)-M(1)-O(3)††	84.45(13)	84.75(24)	84.70(21)	84.69(18)
[2] O(1)-M(1)-O(3)'	95.55(18)	95.25(24)	95.30(21)	95.31(15)
[2] O(1)-M(1)-O(2)††	86.96(15)	87.02(20)	87.23(17)	87.27(15)
[2] O(1)-M(1)-O(2)'	93.04(15)	92.98(20)	92.77(17)	92.73(15)
[2] O(2)-M(1)-O(3)†	104.43(21)	104.77(24)	105.18(21)	105.37(19)
[2] O(2)-M(1)-O(3)††	75.57(21)	75.23(24)	74.82(21)	74.63(19)
M(2) Octahedron				
[2] O(1)-M(2)-O(3)††	91.12(13)	91.16(17)	91.19(15)	91.11(13)
[2] O(1)-M(2)-O(3)'	82.00(13)	81.80(18)	81.91(16)	81.98(14)
[2] O(2)-M(2)-O(3)	96.54(14)	96.60(18)	96.80(16)	96.76(14)
[2] O(2)-M(2)-O(3)††	89.95(14)	90.00(18)	89.74(15)	89.80(14)
[1] O(3)-M(2)-O(3)††	73.21(27)	72.52(34)	72.23(31)	71.91(26)
[2] O(3)-M(2)-O(3)††	89.12(9)	89.12(12)	89.16(11)	89.10(9)
[1] O(3)†-M(2)-O(3)††	108.01(27)	108.68(33)	108.93(29)	109.37(25)
	Monticellite			
	25°C	335°C	615°C	795°C
Tetrahedron				
[1] O(1)-Si-O(2)	115.45(24)	115.70(23)	115.54(27)	115.29(29)
[2] O(1)-Si-O(3)	114.96(16)	114.47(14)	114.49(17)	114.43(18)
[2] O(2)-Si-O(3)†	101.38(17)	102.39(15)	102.36(17)	102.42(18)
[1] O(3)-Si-O(3)††	106.04(29)	105.89(26)	106.11(31)	106.29(33)
M(1) Octahedron				
[2] O(1)-M(1)-O(3)††	87.05(15)	86.80(14)	86.55(16)	86.67(18)
[2] O(1)-M(1)-O(3)'	92.95(15)	93.20(14)	93.45(16)	93.33(18)
[2] O(1)-M(1)-O(2)††	82.88(12)	82.87(12)	82.92(14)	82.95(15)
[2] O(1)-M(1)-O(2)'	97.12(12)	97.13(12)	97.08(14)	97.05(15)
[2] O(2)-M(1)-O(3)†	105.05(16)	105.46(14)	105.68(16)	106.01(16)
[2] O(2)-M(1)-O(3)††	74.95(16)	74.54(14)	74.32(16)	73.99(16)
M(2) Octahedron				
[2] O(1)-M(2)-O(3)††	97.98(12)	97.67(11)	97.39(12)	97.07(12)
[2] O(1)-M(2)-O(3)'	74.36(11)	74.55(11)	74.49(13)	74.52(13)
[2] O(2)-M(2)-O(3)	99.42(13)	99.25(11)	99.41(13)	99.50(13)
[2] O(2)-M(2)-O(3)††	86.20(11)	86.45(10)	86.65(11)	86.86(12)
[1] O(3)-M(2)-O(3)††	65.60(20)	64.94(18)	64.96(21)	64.75(22)
[2] O(3)-M(2)-O(3)††	91.82(9)	91.55(7)	91.35(10)	91.17(11)
[1] O(3)†-M(2)-O(3)††	110.53(19)	111.77(17)	112.12(21)	112.66(22)
	Glaucochroite			
	25°C	300°C	600°C	800°C
Tetrahedron				
[1] O(1)-Si-O(2)	114.71(35)	113.94(36)	114.42(48)	113.40(49)
[2] O(1)-Si-O(3)	114.30(21)	114.21(22)	114.67(27)	114.93(29)
[2] O(2)-Si-O(3)†	103.28(22)	103.65(22)	103.29(29)	103.19(29)
[1] O(3)-Si-O(3)††	105.66(30)	106.01(31)	105.12(40)	105.85(43)
M(1) Octahedron				
[2] O(1)-M(1)-O(3)††	85.46(18)	85.56(19)	85.36(25)	85.86(27)
[2] O(1)-M(1)-O(3)'	94.54(18)	94.44(19)	94.64(25)	94.14(27)
[2] O(1)-M(1)-O(2)††	84.23(18)	84.37(19)	84.02(24)	84.60(24)
[2] O(1)-M(1)-O(2)'	95.77(18)	95.63(19)	95.98(24)	95.40(24)
[2] O(2)-M(1)-O(3)†	107.72(17)	108.32(17)	108.51(23)	108.54(23)
[2] O(2)-M(1)-O(3)††	72.28(17)	71.66(17)	71.49(23)	71.46(23)
M(2) Octahedron				
[2] O(1)-M(2)-O(3)††	95.59(14)	95.44(14)	94.79(17)	94.47(18)
[2] O(1)-M(2)-O(3)'	77.13(16)	77.05(16)	77.07(20)	77.46(21)
[2] O(2)-M(2)-O(3)	99.33(18)	99.61(18)	99.57(23)	99.44(24)
[2] O(2)-M(2)-O(3)††	86.68(13)	86.70(13)	87.31(17)	87.46(18)
[1] O(3)-M(2)-O(3)††	65.19(18)	64.75(19)	64.51(25)	64.08(25)
[2] O(3)-M(2)-O(3)††	89.96(8)	89.80(10)	89.57(12)	89.59(13)
[1] O(3)†-M(2)-O(3)††	114.71(21)	115.42(22)	116.05(28)	116.41(30)

*The numbers in brackets refer to the multiplicity of the angle.

†Angle opposite O-O edge shared between an octahedron and tetrahedron.

‡Angle opposite O-O edge shared between two octahedra.

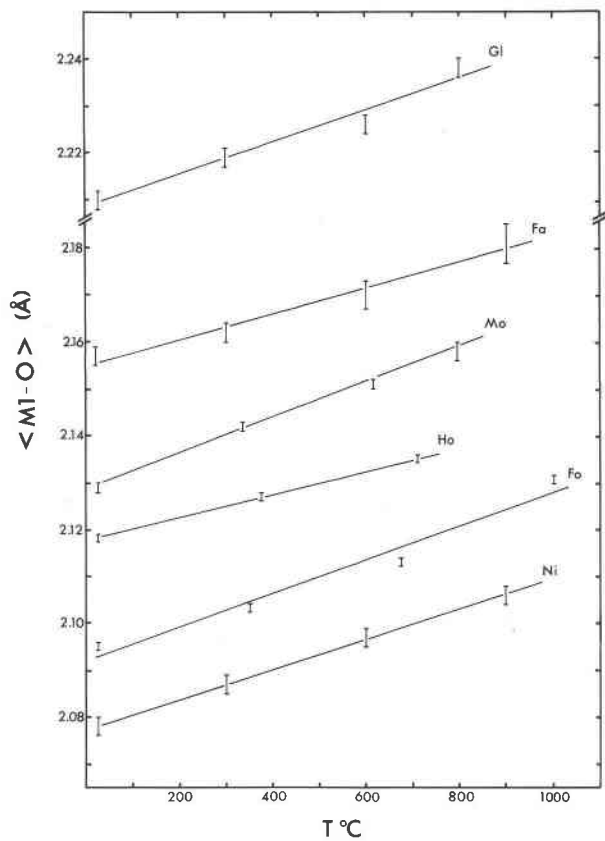


Fig. 2. Plot of the mean $M(1)$ -O distances versus temperature for Ni-olivine (Ni), forsterite (Fo), hortonolite (Ho), fayalite (Fa), monticellite (Mo), and glaucochroite (Gl). Error bars refer to one estimated standard deviation.

$M(2)$ cation displacement

With increasing temperature, the $M(2)$ cation is displaced from the centroid of the octahedron in a direction away from the triangle of shared edges (Fig. 1). Cation displacements with temperature have also

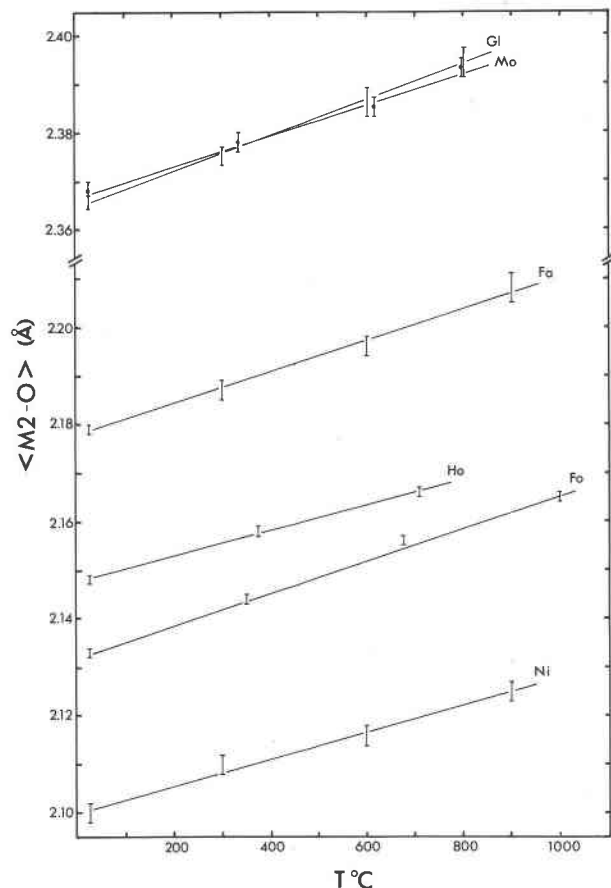


Fig. 3. Plot of the mean $M(2)$ -O distances versus temperature for six olivines. Unless otherwise stated, the abbreviations in this and subsequent figures are the same as those in Fig. 2.

been noted in the $M(2)$ polyhedron in pyroxenes and the $M(4)$ polyhedron in amphiboles (Cameron *et al.*, 1973; Sueno *et al.*, 1973). In this study, the rate of change of displacement with temperature decreases in the order Mo ~ Fo ~ Gl > Ni > Fa ~ Ho (Fig. 4 and Table 10).

Table 9. Linear thermal expansion coefficients ($^{\circ}\text{C}^{-1} \times 10^6$) of mean M-O distances and unit-cell parameters in six olivines

Olivine	$\langle M(1)-O \rangle$	$\langle M(2)-O \rangle$	a	b	c
Ni-Olivine	1.54(2)*	1.31(10)	1.18(5)	1.09(4)	1.11(3)
Forsterite	1.93(24)**	1.72(8)	0.87(11)**	1.54(2)**	1.33(2)**
Hortonolite	1.17(2)	1.22(7)	0.61(1)	0.96(7)	0.97(10)
Fayalite	1.26(13)	1.50(9)	0.99(8)	0.95(9)	1.19(9)
Monticellite	1.74(5)	1.33(9)	1.01(8)	0.99(2)	1.13(4)
Glaucochroite	1.54(20)	1.52(4)	0.87(11)	1.02(3)	1.45(8)

* The value of r^2 for the regressions ranged from 0.95 to 0.99.

** Data fit to simple linear equation for comparative purposes.

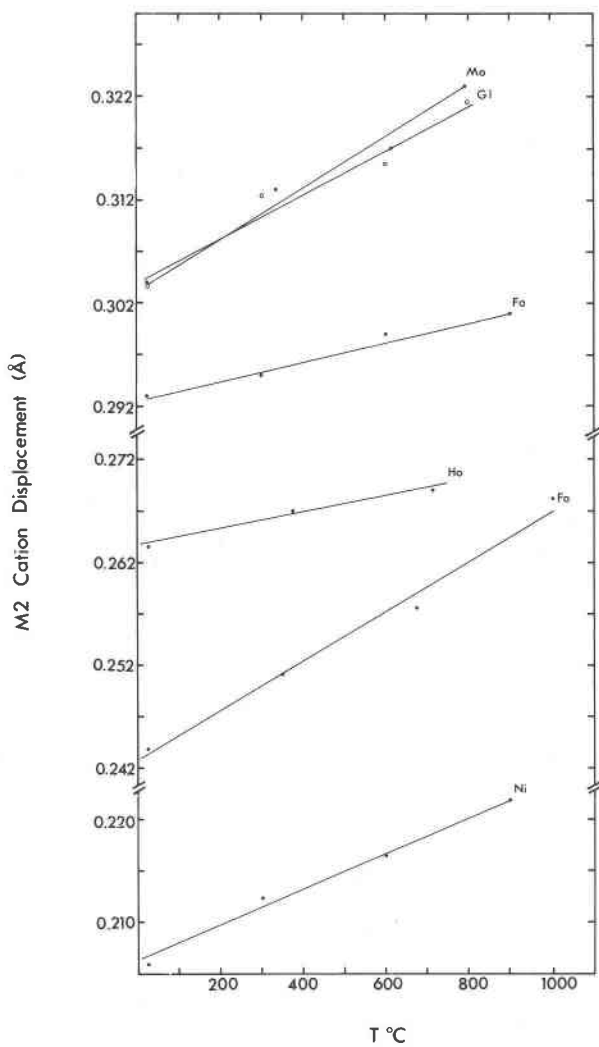


Fig. 4. Plot of the displacement of the $M(2)$ cation from the centroid of the octahedron versus temperature for six olivines.

Figure 5 indicates that in the room-temperature structures the magnitude of displacement increases with increasing cation radius. The room-temperature position of the cation in the $M(4)$ site in amphibole and the $M(2)$ site in pyroxene is also related to the radius of the cation (Papike *et al.*, 1969; Takeda, 1972). The displacement at room temperature as a function of $M(2)$ cation radius may be explained qualitatively as resulting from the asymmetric distribution of shared edges about the $M(2)$ octahedron. For example, increasing the effective radius of the $M(2)$ cation from Ni^{2+} (0.70 \AA ; Shannon and Prewitt, 1969) in Ni_2SiO_4 to Ca^{2+} (1.00 \AA) in Ca_2SiO_4 results in an insignificant increase in the shared edge $\text{O}(3)-\text{O}(3')$, whereas the opposite unshared edge $\text{O}(3'')-\text{O}(3''')$ increases from 3.304 to 4.116 \AA (Brown, 1970).

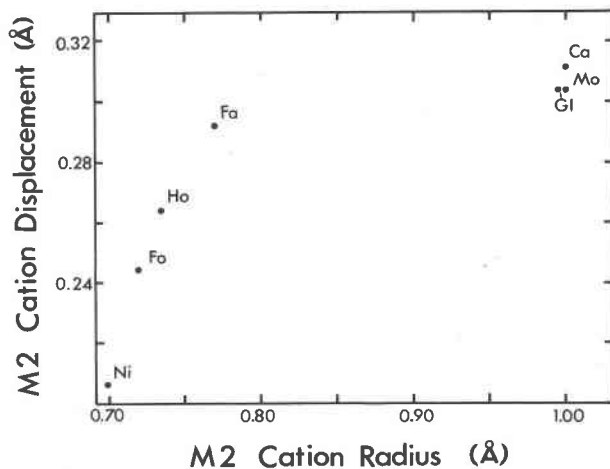


Fig. 5. Plot of the room temperature displacement of the $M(2)$ cation from the centroid of the octahedron versus $M(2)$ cation radius for seven olivine structures. The abbreviation Ca refers to $\gamma\text{-Ca}_2\text{SiO}_4$ (Brown, 1970). Cation radii are from Shannon and Prewitt (1969).

This, coupled with an increased $M(2)$ -O distance, results in a shift of the $M(2)$ cation away from the shared edge and the centroid of coordinating oxygens.

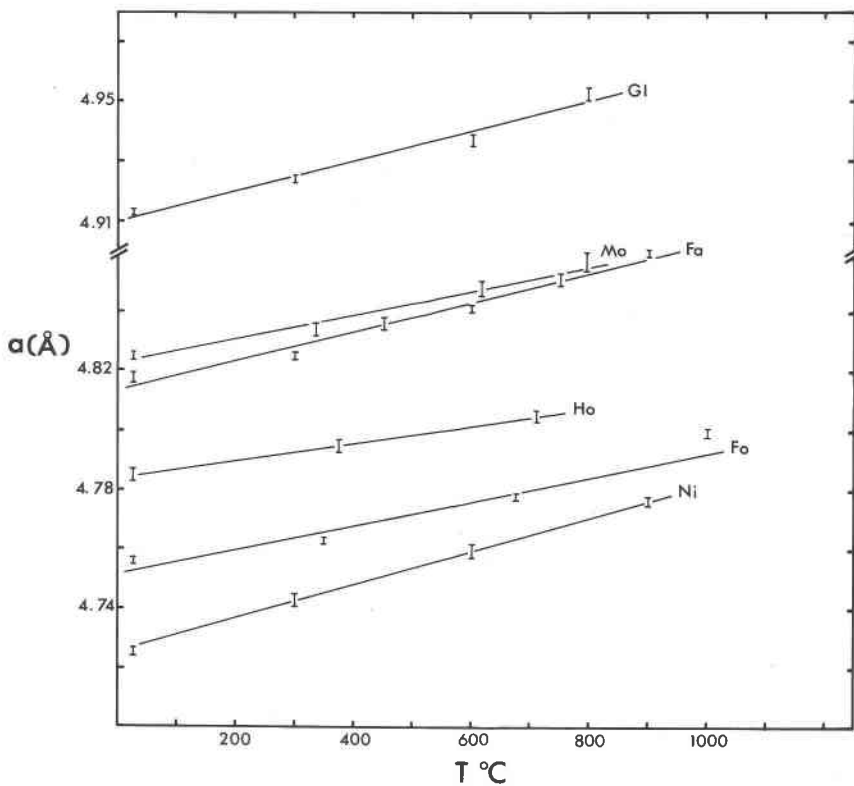
Thermal parameters

For a given structure, the rate of increase in B is greater for the M cations than Si cations (Table 4).

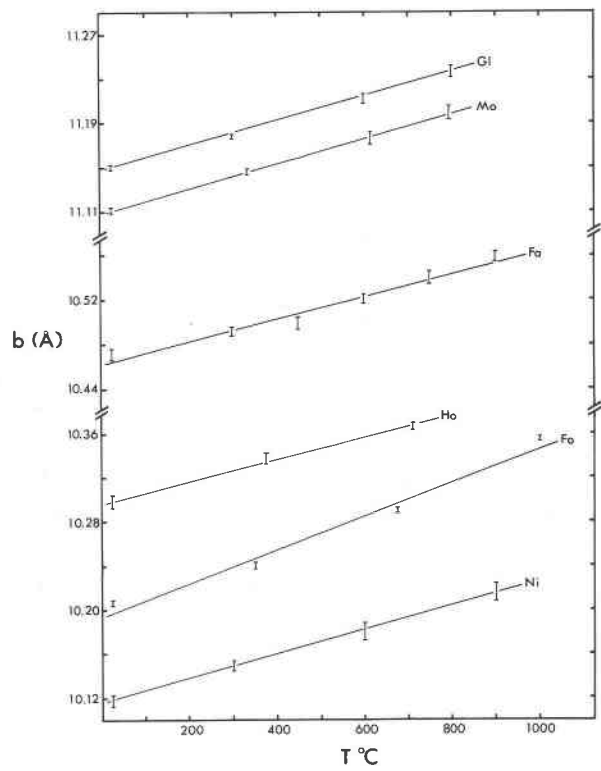
Table 10. Magnitude (A) and rate of increase ($\text{A}/^\circ\text{C} \times 10^5$) of the displacement of the $M(2)$ cation with increasing temperature for six olivines

Olivine	Displacement	Olivine	Displacement
Ni-Olivine	Δ	Hortonolite	Δ
25°	0.206	24°	0.264
300°	0.212	375°	0.267
600°	0.217	710°	0.269
900°	0.222		
$d\Delta/dT$	1.79(13)		0.81(18)
Forsterite		Fayalite	
25°	0.244	20°	0.293
350°	0.251	300°	0.295
675°	0.258	700°	0.299
1000°	0.268	900°	0.301
$d\Delta/dT$	2.44(19)		0.95(19)
Monticellite		Glaucophroite	
25°	0.304	25°	0.304
335°	0.313	300°	0.312
615°	0.317	600°	0.316
795°	0.323	800°	0.321
$d\Delta/dT$	2.35(23)		2.14(31)

* The displacement of the $M(2)$ cation in $\gamma\text{-Ca}_2\text{SiO}_4$ (Brown, 1970) at 25°C is 0.311 Å.

Fig. 6. Plot of the a cell edge versus temperature for six olivines.

The anisotropic thermal vibration ellipsoids for $M(1)$, $M(2)$, and Si atoms in Ni-olivine, monticellite, and glaucochroite are generally triaxial. With heating, they increase in size but maintain approximately the same shape. Brown and Prewitt (1973) suggested that the shape of the thermal ellipsoid for the $M(2)$ cation in hortonolite at high temperatures was, in part, related to the effects of positional disorder. As discussed in the previous section, the temperature dependence of the cation position in the $M(2)$ octahedron varies from structure to structure. For example, the Mg^{2+} cation (forsterite) exhibits a much larger rate of displacement with temperature than the Fe^{2+} cation (fayalite). Because the displacement is primarily along $+b$, one would expect the Mg^{2+} and Fe^{2+} cations in hortonolite to occupy increasingly different mean positions along b with increasing temperature relative to their positions at room temperature. This will tend to increase the magnitude of the apparent thermal ellipsoid parallel to b . Brown and Prewitt (1973) noted a decrease in the anisotropy of the thermal ellipsoid for $M(2)$ as a function of temperature, which was primarily due to an increase in the magnitude of the ellipsoid axis parallel to b . The effects of positional disorder on the shapes of the thermal ellip-

Fig. 7. Plot of the b cell edge versus temperature for six olivines.

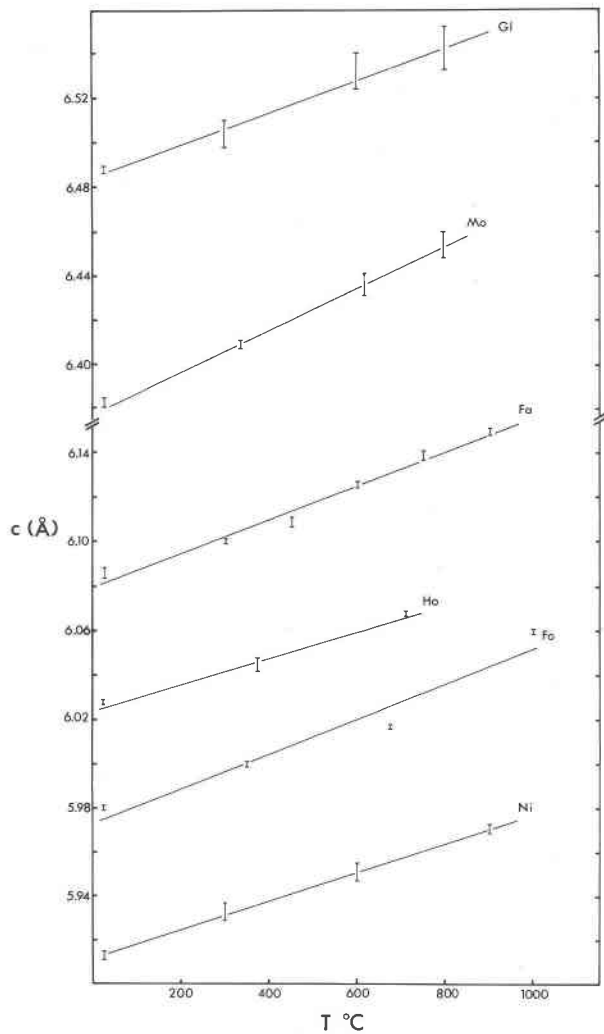


Fig. 8. Plot of the *c* cell edge versus temperature for six olivines.

soids in pyroxenes and amphiboles have been discussed by Cameron *et al.* (1973).

The thermal ellipsoids for the oxygen atoms in all structures are triaxial and do not vary appreciably in orientation with increasing temperature. In general, the shortest axes of the ellipsoids are oriented parallel to the associated Si-O bond.

Unit cell expansions

With the possible exception of forsterite, unit-cell parameters exhibit a simple linear relationship with temperature (Figs. 6, 7, and 8; Table 11). A comparison of linear thermal expansion coefficients (Table 9) indicates the following relationships: (1) $\alpha_a \sim \alpha_b \sim \alpha_c$ for Ni-olivine, (2) α_c increases relative to α_b in the (Mg,Fe) olivines with increasing Fe content, and (3) $\alpha_c > \alpha_b, \alpha_a$ for the Ca-olivines.

M(1) octahedra and Si tetrahedra share two O(2)-O(3) edges oriented with their largest vector component parallel to *b*. Because the length of these edges remains essentially constant with temperature, the smallest expansion in *M*(1) is parallel to *b*. As a result, *b* cell-edge expansion in olivines is controlled primarily by expansions in *M*(2) octahedra. The relationship of polyhedral expansion to *a* and *c* cell-edge expansion is more difficult to rationalize.

Structural control of olivine melting

Hazen (1977) has observed that structural parameters (*i.e.* unit-cell edges and mean *M*-O distances) of forsterite, hortonolite, and fayalite are very similar at the melting point of each olivine. On this basis, he has suggested that the breakdown of olivine to a melt may be related to the structural misfit between octa-

Table 11. Unit-cell dimensions (Å) and volumes (Å³) for Ni-olivine, monticellite, and glaucochroite

Olivine	T (°C)	<i>a</i> (Å)	<i>b</i> (Å)	<i>c</i> (Å)	<i>V</i> (Å ³)
Ni-Olivine	25	4.726(1)	10.118(2)	5.913(1)	282.8(1)
	300	4.744(1)	10.151(2)	5.933(2)	285.7(1)
	600	4.760(3)	10.179(4)	5.951(3)	288.3(3)
	900	4.775(1)	10.216(2)	5.971(3)	291.3(2)
Monticellite	25	4.825(1)	11.111(1)	6.383(2)	342.2(1)
	335	4.834(1)	11.147(2)	6.409(2)	345.4(1)
	615	4.848(2)	11.176(6)	6.436(5)	348.7(4)
	795	4.857(3)	11.199(6)	6.454(6)	351.1(4)
Glaucochroite	25	4.913(1)	11.151(2)	6.488(1)	355.4(1)
	300	4.924(1)	11.178(2)	6.504(6)	358.0(3)
	600	4.937(2)	11.212(4)	6.532(8)	361.6(5)
	800	4.953(2)	11.237(5)	6.543(10)	364.2(6)

hedra and tetrahedra. Octahedra expand with heating to a critical limit governed by the size of the smaller, rigid tetrahedra. Beyond this limit, structural weaknesses develop as a result of shared-edge misfit and melting occurs. Because the dimensions of the tetrahedra remain essentially constant as a function of both composition (Brown, 1970) and temperature, the sizes of the octahedra at melting are predicted to be the same in all olivines.

Linear extrapolation of unit-cell expansion data to the melting points of Ni_2SiO_4 and Co_2SiO_4 (Pistorius, 1963) results in cell volumes of 299 \AA^3 and 310 \AA^3 , respectively, which are significantly less than that calculated for Mg-Fe olivines ($\sim 319 \text{ \AA}^3$). The approximate volumes of $M(1)$ and $M(2)$ octahedra in Ni_2SiO_4 at melting are 12.3 \AA^3 ($(M(1)-\text{O}) = 2.13 \text{ \AA}$) and 12.7 \AA^3 ($(M(2)-\text{O}) = 2.15 \text{ \AA}$), respectively (compared to volumes of $\sim 13 \text{ \AA}^3$ and $\sim 14 \text{ \AA}^3$ for Mg-Fe olivines). Apparently other factors, in addition to shared-edge misfit, account for the instability of Ni_2SiO_4 .

The approximate volumes of $M(1)$ and $M(2)$ octahedra in monticellite and glaucochroite at melting are 13.2 \AA^3 and 17.4 \AA^3 and 14.2 \AA^3 and 17.2 \AA^3 , respectively. In view of the size of the larger $M(2)$ octahedron, it is interesting to note the similarity between the extrapolated volume of $M(1)$ in monticellite and the Mg-Fe olivines at melting. This similarity may be coincidental and, in any case, is not consistent with the $M(1)$ octahedral volume in Ni_2SiO_4 at melting. A proper evaluation of these relations is precluded by current understanding of the nature of chemical bonding in olivines.

Acknowledgments

Dr. G. V. Gibbs of the Department of Geological Sciences at Virginia Polytechnic Institute and State University read an earlier version of the manuscript and made several helpful suggestions for its improvement. Thanks are also extended to Dr. G. E. Brown of Stanford University for providing samples of Ni-olivine and glaucochroite. This research was supported by the National Research Council through grant 67-7061.

References

- Bence, A. E. and A. L. Albee (1968) Empirical correction factors for the electron microanalysis of silicates and oxides. *J. Geol.*, **76**, 382-403.
- Birle, J. D., G. V. Gibbs, P. B. Moore and J. V. Smith (1968) Crystal structures of natural olivines. *Am. Mineral.*, **53**, 807-824.
- Bragg, W. L. and G. B. Brown (1926) Die Struktur des Olivins. *Z. Kristallogr.*, **63**, 538-556.
- Brown, G. E. (1970) *Crystal Chemistry of the Olivines*. Ph.D. Thesis, Virginia Polytechnic Institute and State University, Blacksburg, Virginia.
- and C. T. Prewitt (1973) High-temperature crystal chemistry of hortonolite. *Am. Mineral.*, **58**, 577-587.
- Busing, W. R., K. O. Martin and H. A. Levy (1962) ORFFE: A Fortran crystallographic least-squares refinement program. *US Clearinghouse Fed. Sci. Tech. Info. Doc., ORNL-TM-305*.
- Cameron, M., S. Sueno, C. T. Prewitt and J. J. Papike (1973) High-temperature crystal chemistry of acmite, diopside, hedenbergite, jadeite, spodumene and ureyite. *Am. Mineral.*, **58**, 594-618.
- Cruickshank, D. W. J. (1965) Errors in least-squares methods. In J. S. Rollett, Ed., *Computing Methods in Crystallography*. Pergamon Press, New York.
- Doyle, P. A. and P. S. Turner (1968) Relativistic Hartree-Fock X-ray and electron scattering factors. *Acta Crystallogr.*, **A24**, 390-397.
- Foit, F. F. and D. R. Peacor (1967) A high temperature furnace for a single crystal X-ray diffractometer. *J. Sci. Instrum.*, **44**, 183-185.
- Ghose, S. and C. Wan (1974) Strong site preference of Co^{+2} in olivine, $\text{Co}_{1.10}\text{Mg}_{0.90}\text{SiO}_4$. *Contrib. Mineral. Petrol.*, **47**, 131-140.
- Hazen, R. M. (1976) Effects of temperature and pressure on the crystal structure of forsterite. *Am. Mineral.*, **61**, 1280-1293.
- (1977) Effects of temperature and pressure on the crystal structure of ferromagnesium olivine. *Am. Mineral.*, **62**, 286-295.
- Hamilton, W. C. (1959) On the isotropic temperature factor equivalent to a given anisotropic temperature factor. *Acta. Crystallogr.*, **12**, 609-610.
- Lager, G. A., and E. P. Meagher (1975) Strain analysis of polyhedral distortions in olivines at high temperatures (abstr.). *Geol. Soc. Am. Abstr. Programs*, **7**, 1158.
- Meagher, E. P. (1975) The crystal structures of pyrope and grossularite at elevated temperatures. *Am. Mineral.*, **60**, 218-228.
- Papike, J. J., M. Ross and J. R. Clark (1969) Crystal-chemical characterization of clinoamphiboles based on five new structure refinements. *Mineral. Soc. Am. Spec. Pap.*, **2**, 117-136.
- Pistorius, C. W. F. T. (1963) Some phase relations in the systems $\text{CoO}-\text{SiO}_2-\text{H}_2\text{O}$, $\text{NiO}-\text{SiO}_2-\text{H}_2\text{O}$ and $\text{ZnO}-\text{SiO}_2-\text{H}_2\text{O}$ to high pressures and temperatures. *Neues Jahrb. Mineral. Monatsh.*, **21-57**.
- Rajamani, V., G. E. Brown and C. T. Prewitt (1975) Cation ordering in Ni-Mg olivine. *Am. Mineral.*, **60**, 292-299.
- Shannon, R. D. and C. T. Prewitt (1969) Effective ionic radii in oxides and fluorides. *Acta Crystallogr.*, **B25**, 925-946.
- Smyth, J. R. (1975) High temperature crystal chemistry of fayalite. *Am. Mineral.*, **60**, 1092-1097.
- and R. M. Hazen (1973) The crystal structures of forsterite and hortonolite at several temperature up to 900°C . *Am. Mineral.*, **58**, 588-593.
- Sueno, S., M. Cameron, J. J. Papike and C. T. Prewitt (1973) High-temperature crystal chemistry of tremolite. *Am. Mineral.*, **58**, 649-664.
- Takeda, H. (1972) Crystallographic studies of coexisting aluminan orthopyroxene and augite of high pressure origin. *J. Geophys. Res.*, **77**, 5798-5811.
- Wenk, H. R. and K. N. Raymond (1973) Four new structure refinements of olivine. *Z. Kristallogr.*, **137**, 86-105.